scientific reports

Check for updates

OPEN

High-content analysis of proteostasis capacity in cellular models of amyotrophic lateral sclerosis (ALS)

Isabella A. Lambert-Smith[1,2]✉, Victoria K. Shephard[1,2], Luke McAlary[1,2], Justin J. Yerbury[1,2] & Darren N. Saunders[1]✉

Disrupted proteome homeostasis (proteostasis) in amyotrophic lateral sclerosis (ALS) has been a major focus of research in the past two decades. However, the proteostasis processes that become disturbed in ALS are not fully understood. Obtaining more detailed knowledge of proteostasis disruption in association with different ALS-causing mutations will improve our understanding of ALS pathophysiology and may identify novel therapeutic targets and strategies for ALS patients. Here we describe the development and use of a novel high-content analysis (HCA) assay to investigate proteostasis disturbances caused by the expression of several ALS-causing gene variants. This assay involves the use of conformationally-destabilised mutants of firefly luciferase (Fluc) to examine protein folding/re-folding capacity in NSC-34 cells expressing ALS-associated mutations in the genes encoding superoxide dismutase-1 ($SOD1^{A4V}$) and cyclin F ($CCNF^{S621G}$). We demonstrate that these Fluc isoforms can be used in high-throughput format to report on reductions in the activity of the chaperone network that result from the expression of $SOD1^{A4V}$, providing multiplexed information at single-cell resolution. In addition to $SOD1^{A4V}$ and $CCNF^{S621G}$, NSC-34 models of ALS-associated TDP-43, FUS, UBQLN2, OPTN, VCP and VAPB mutants were generated that could be screened using this assay in future work. For ALS-associated mutant proteins that do cause reductions in protein quality control capacity, such as $SOD1^{A4V}$, this assay has potential to be applied in drug screening studies to identify candidate compounds that can ameliorate this deficiency.

Keywords Amyotrophic lateral sclerosis, Cyclin F, Neurodegeneration, Proteostasis, Superoxide dismutase-1

Post-mortem examination of spinal cord tissue from amyotrophic lateral sclerosis (ALS) patients consistently reveals the presence of TDP-43-, FUS- or SOD1- and ubiquitin-positive inclusions comprised of insoluble proteinaceous material[1–4]. Misfolded proteins, as either abnormal monomers and/or oligomeric precursors, possess cytotoxic properties[5–7] and their aggregation into certain kinds of inclusions may serve to protect cells and to assist in the clearance of these toxic species[8–17]. There is strong evidence that the progressive spread of pathology in patients could be due to the cell-to-cell propagation of protein misfolding and aggregation[18,19]. However, the formation of protein inclusions is also indicative of dysregulated proteome homeostasis (proteostasis)[20,21] and the inability of the cell to properly monitor, refold or degrade non-native proteins.

Many of the ALS-associated genes encode proteins with functional roles in the maintenance of proteostasis in cells, or that are aggregation-prone, or that, in their mutant form, cause dysfunction of components of proteostasis machinery[22]. For instance, in addition to the presence of ubiquitylated SOD1 inclusions in post-mortem tissue from ALS patients[23], there is extensive evidence documenting correlations between mutant SOD1 aggregation, chaperone activity modulation and decreases in ubiquitin–proteasome system (UPS) activity[24–30]. ALS-associated ubiquilin-2 (UBQLN2), VAMP (vesicle-associated membrane protein)-associated protein B (VAPB), optineurin (OPTN), cyclin F (CCNF) and transitional endoplasmic reticulum ATPase/p97 (VCP) each have roles in protein degradation pathways, encoding components of the UPS or autophagy machinery[31–37].

TDP-43 is one of the major protein constituents of ubiquitylated inclusions in sporadic ALS, which comprises ~90% of all ALS cases[38]. Mutations in a highly conserved region of the *TARDBP* gene occur in both familial and

[1]Illawarra Health and Medical Research Institute, University of Wollongong, Wollongong, NSW 2522, Australia. [2]Molecular Horizons and School of Chemistry and Molecular Bioscience, University of Wollongong, Wollongong, NSW 2522, Australia. ✉email: ilsmith@uow.edu.au; dnsaunders@icloud.com

Figure 1. Schematic of High Content Analysis (HCA) image processing and analysis optimisation. To analyse the fluorescence intensity of EGFP-/tGFP- and tdTomato (tdT)/mCherry-fusion proteins and quantify protein inclusions containing fluorescent fusion proteins in NSC-34 cells, we deployed the Spot Detector BioApplication designed to analyse fluorescent foci in cells. Optimisation was carried out using images of NSC-34 cells triple-transfected to express H2B-ECFP, either $SOD1^{WT}$-EGFP, $SOD1^{A4V}$-EGFP, TDP-43^{WT}-tGFP TDP-43^{M337V}-tGFP, FUS^{WT}-tGFP, FUS^{R495X}-tGFP, FUS^{R521G}-tGFP or EGFP alone and mCherry alone. Cells were imaged at 48 h post-transfection using a 20 × objective lens. (**a**) Raw images from Channels 1 (H2B-ECFP), 2 (EGFP-/tGFP-fusion proteins) and 3 (tdT/mCherry-fusion proteins) were first pre-processed to remove background fluorescence, exclude cells positioned on the border of each image from analysis and distinguish individual cells ('object' segmentation). Channel 1 images were additionally smoothed (blurred) to help reduce fluorescent noise that could lead to the false inclusion of image artefacts in subsequent analyses. (**b**) Biological 'objects', in this case cells, were identified using nuclear-localised H2B-ECFP fluorescence in Channel 1 images. To select viable transfected cells for analysis and exclude image artefacts, dead cells and cell debris, cells were selected based on the size and fluorescence intensity of their ECFP-fluorescent nuclei. (**c**) The relevant measures for GFP fluorescence intensity and fluorescent foci were measured in Channel 2 within a circular analysis mask that expanded the mask derived in Channel 1. The green circular mask indicates cells selected for analysis, while yellow masks indicate fluorescent foci/'spots' selected for analysis. To detect and analyse fluorescent foci corresponding to protein inclusions, upper and lower limits for size and fluorescence intensity were set. (**d**) Channel 3 objects were identified using the same mask as Channel 2.

sporadic ALS patients[39]. Mutations in another DNA/RNA-binding protein, FUS, occur in ~4–5% of familial ALS patients[3,4]. Unlike the majority of ALS cases, FUS familial ALS cases are associated with the presence of cytoplasmic inclusions that do not show immunoreactivity for TDP-43, but are positive for FUS[40]. Indeed, TDP-43, FUS and SOD1 have been demonstrated to form distinct types of inclusions via divergent pathways in cells[41]. TDP-43 and FUS each have several thousand mRNA targets[42–44]. TDP-43 deficiency has been found to affect the levels of mRNAs encoding OPTN, VAPB and VCP, all of which, as already mentioned, are implicated in ALS and have critical roles in protein degradation pathways[43]. FUS has also been reported to bind to mRNAs encoding OPTN, VAPB, VCP and UBQLN2, as well as mRNAs encoding other proteins involved in the UPS[42,45,46]. Dysregulation of TDP-43 and FUS can lead to consequent abnormalities in mRNA splicing and processing, and cytoplasmic accumulations of TDP-43 and FUS may aberrantly sequester RNAs and other proteins, causing further dysfunction in cellular RNA metabolism and disruptions in the activities of the affected target proteins[42,47].

Although we can identify that proteostasis dysfunction in motor neurons may be an underlying pathogenic link between the different ALS-associated genetic mutations, there remains a need to identify the exact proteostasis disruptions that are commonly associated with each of the ALS-causing genetic mutations, and those that are unique to each gene variant. Given the genetic and functional heterogeneity of ALS, the development of high-content analysis (HCA) assays that can measure multiple phenotypic features in cellular ALS models and extract rich, descriptive information of responses to candidate therapeutic compounds and modifiers of ALS gene toxicity will be valuable. Assays that utilise the principles of HCA could help to facilitate rapid discovery of common and unique proteostasis disruptions amongst the different aetiologies of ALS. In the past 20 years, HCA approaches have evolved to emerge as attractive options for researchers interested in obtaining extensively descriptive phenotypic data through automated microscopy. To address the need for efficient HCA screening platforms to interrogate disease mechanisms across genetically-diverse ALS models, we have developed an experimental system with HCA capacity that can be used to extract multiplexed phenotypic data from cellular ALS models. In the present work we have tested this system to examine proteostasis capacity in cellular models of SOD1- and CCNF-linked ALS. Our data demonstrate that conformationally-destabilised mutants of firefly luciferase (Fluc) can be used in high-throughput format as a tool to measure cellular protein folding/re-folding capacity in cellular models of ALS-associated mutants. Applying this assay in high-throughput format provides the advantage of speed, combined with the capacity to gain single-cell resolution information about cellular phenotype using multiple readouts from the HCA platform.

Materials and methods

Plasmids

All plasmids are detailed in the Supplementary Material.

Cell culture

NSC-34 cells[48] were maintained in 10% (v/v) fetal bovine serum (FBS; Bovogen Biologicals) in Dulbecco's Modified Eagle's Medium/Ham's Nutrient Mixture F-12 (DMEM/F-12). Cells were seeded into either 8-well µ-Slides (Ibidi) for confocal microscopy or 96-well plates (Greiner Bio-One) for imaging using the Cellomics ArrayScan VTI imaging platform (Thermo Scientific). After overnight incubation at 37 °C under 5% CO_2/95% air, cells were either single-transfected or triple-transfected (detailed in Tables S1 and S2, supplementary information) using Lipofectamine 2000 (Invitrogen) according to manufacturer's instructions. For triple transfections, plasmids were used at a 1:1:1 ratio. All transfection conditions were carried out in quadruplicate. For experiments involving proteasome inhibition, MG132 was solubilised in DMSO at 20 mM and subsequently diluted to 5 µM in 10% (v/v) FBS in DMEM/F-12. The prepared solution was added to cells 30 h post-transfection and incubated for 18 h.

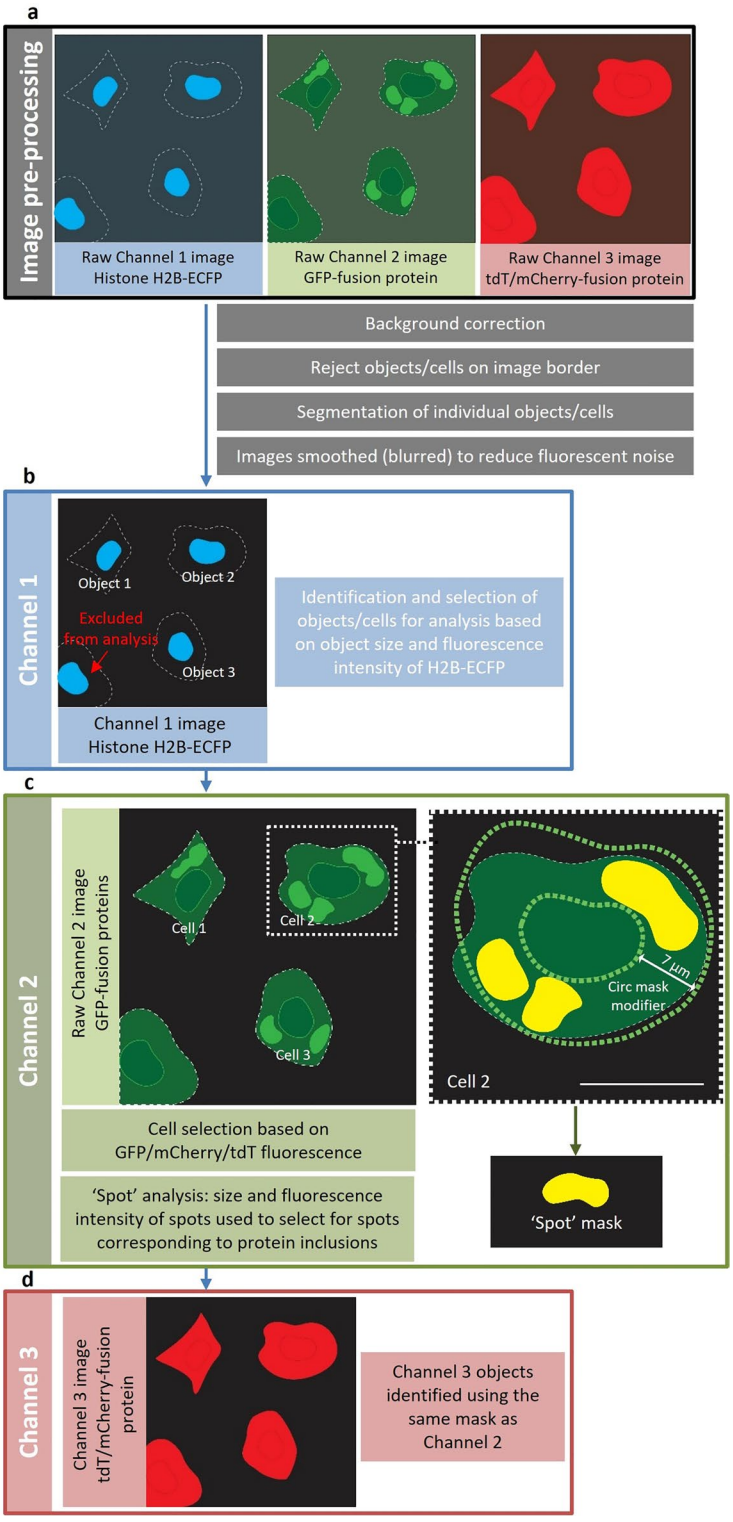
a
Image pre-processing
Raw Channel 1 image
Histone H2B-ECFP
Raw Channel 2 image
GFP-fusion protein
Raw Channel 3 image
tdT/mCherry-fusion protein
Background correction
Reject objects/cells on image border
Segmentation of individual objects/cells
Images smoothed (blurred) to reduce fluorescent noise
b
Channel 1
Object 1
Object 2
Excluded from analysis
Object 3
Channel 1 image
Histone H2B-ECFP
Identification and selection of objects/cells for analysis based on object size and fluorescence intensity of H2B-ECFP
c
Channel 2
Raw Channel 2 image
GFP-fusion proteins
Cell 1
Cell 2
Cell 3
7 µm
Circ mask modifier
Cell 2
Cell selection based on GFP/mCherry/tdT fluorescence
'Spot' analysis: size and fluorescence intensity of spots used to select for spots corresponding to protein inclusions
'Spot' mask
d
Channel 3
Channel 3 image
tdT/mCherry-fusion protein
Channel 3 objects identified using the same mask as Channel 2

Confocal microscopy

Localisation of each fusion protein in transfected NSC-34 cells was characterised by imaging using a TCS SP5 II confocal microscope with a 63 × oil-immersion objective lens (Leica Microsystems). Imaging was carried out 48 h post-transfection.

High-content analysis

NSC-34 cells were imaged either live or fixed (in 4% (w/v) paraformaldehyde for 20 min at room temperature) using the 20 × objective of a Cellomics ArrayScan VTI imaging platform (Thermo Scientific). All assays described are appropriate for either live or fixed cell imaging. Fluorescence of ECFP-, EGFP- and tdT/mCherry-fusion proteins was imaged using excitation filters of 386 nm, 485 nm and 549 nm, respectively. Phase contrast and fluorescent images from 20 fields of view per well were acquired, with image analysis parameters optimised using the SpotDetector V4 BioApplication in HCS Studio (Thermo Scientific) summarised in Fig. 1 (further detail in Figure S1). Primary object identification was based on expression of H2B-ECFP in channel 1, while GFP or tdTomato/mCherry-fusion proteins were detected in channels 2 and 3.

Results

Characterisation of cellular ALS models

Given the extraordinary molecular heterogeneity of ALS, we developed a suite of ALS models representing genetically diverse fALS aetiologies in NSC-34 cells by expressing EGFP-/tGFP-/mCherry-fusions of mutant SOD1, TDP-43, FUS, CCNF, UBQLN2, OPTN, VCP or VAPB. The genetic mutations for these models were selected after careful consideration of the mutations that segregate with ALS; *SOD1*^{A4V}[49], *TARDBP*^{M337V}[50], *FUS*^{R495X}, *FUS*^{R521G}[3,4], *CCNF*^{S621G}[37], *UBQLN2*^{P497H}[33], *OPTN*^{E478G}[34], *VAPB*^{P56S}[36], *VCP*^{R159H} and *VCP*^{R191Q}[32]. Prior to using these NSC-34 models in an HCA format, we first characterised the expression (via immunoblot), localisation, toxicity, and solubility of each WT and mutant fusion protein (Figs. 2 and S3–S9). Importantly, EGFP and mCherry were diffusely distributed throughout the cell and did not aggregate (Figure S2a, i and b, i). It was also confirmed that the expression of EGFP or mCherry-alone had no effect on cell viability (Figure S2a, ii and b, ii).

Toxicity of mutant SOD1, TDP-43, FUS and CCNF

Live cell imaging of cells expressing SOD1^{WT}-EGFP and SOD1^{A4V}-EGFP to monitor cell population growth showed that the numbers of cells expressing SOD1^{WT}-EGFP and EGFP-alone steadily increased, while the numbers of cells expressing SOD1^{A4V}-EGFP increased at a slower rate (Fig. 2a, iv). At 48 h post-replating there were significantly lower numbers of cells expressing SOD1^{A4V}-EGFP than SOD1^{WT}-EGFP ($p = 0.0151$) (Fig. 2a, v). This indicates that the overexpression of SOD1^{A4V}-EGFP caused toxicity.

A similar trend was observed for cells expressing TDP-43, FUS or CCNF. Comparison of the mean numbers of GFP/RFP-positive transfected cells at 72 h post-transfection showed that there was a significantly greater number of cells expressing WT proteins than cells expressing mutants (TDP-43^{M337V}-tGFP, $p < 0.001$; FUS^{R495X}-tGFP, $p = 0.0014$; FUS^{R521G}-tGFP, $p = 0.0023$; CCNF^{S621G}-mCherry, $p < 0.0001$) (Fig. 2b–d, v).

Localisation and aggregation of mutant SOD1, TDP-43, FUS and CCNF

Inclusions of ALS-associated proteins are generally 2–20 µm in diameter in both human post-mortem tissue[34,51–54] and in cell culture models[27,55–59]. A size minimum of 2 µm was thus established as suitable for categorising fluorescent foci as inclusions. The foci formed by SOD1^{A4V}-EGFP, TDP-43^{M337V}-tGFP, FUS^{R495X}-tGFP, FUS^{R521G}-tGFP and CCNF^{S621G}-mCherry were manually examined in images of cells and were consistently measured to be larger than 2 µm (Fig. 2a, i–d, i).

While SOD1^{WT}-EGFP was observed to have a relatively even distribution throughout the cytoplasm and within nuclei, in a proportion of cells SOD1^{A4V}-EGFP formed multiple large inclusions in the cytoplasm (Fig. 2a, i). Saponin-permeabilisation[60] showed that there was no fluorescent signal from cells overexpressing SOD1^{WT}-EGFP following permeabilisation, indicating that SOD1^{WT}-EGFP remained soluble in all cells that were imaged (Fig. 2a, ii and iii). In accordance with the confocal microscopy data, a significantly greater percentage of cells (10.38 ± 0.27%) expressing SOD1^{A4V}-EGFP remained EGFP-positive following permeabilisation ($p < 0.0001$), indicating that SOD1^{A4V}-EGFP was present in an insoluble, non-diffusable form in a proportion of cells.

Imaging transfected cells using confocal microscopy, it was observed that TDP-43^{WT} and FUS^{WT} remained localised to cell nuclei, while the TDP-43 and FUS mutants mislocalised to the cytoplasm and formed large aggregates and smaller foci, as is observed in ALS patient tissue (Fig. 2b, i and c, i)[3,4,50]. Although TDP-43^{WT}-tGFP was not observed to mislocalise and accumulate into cytoplasmic inclusions when cells were examined using confocal microscopy, TDP-43^{WT}-tGFP was found to remain inside 55.22 ± 0.69% of transfected cells after plasma membrane permeabilisation (Fig. 2b, ii). However, a significantly greater percentage of cells expressing TDP-43^{M337V}-tGFP were tGFP-positive following permeabilisation (79.41 ± 2.18%) compared to cells expressing TDP-43^{WT}-tGFP ($p = 0.0035$). TDP-43^{WT}-tGFP within the nucleus may not have been released when cells were incubated with saponin solution. TDP-43 binds DNA and RNA in the nucleus, which causes it to become retained even within permeabilised cells[61,62]. In this case, the saponin-permeabilisation assay may not be appropriate for assaying the formation of cytoplasmic TDP-43 inclusions, as the automated live cell imaging capabilities used in this assay may not allow for distinction between nuclear TDP-43 and cytoplasmic inclusions. To evaluate this, a time-resolved saponin-permeabilisation assay was performed, in which transfected cells were imaged prior to saponin-permeabilisation and then at 5, 10 and 15 min following the addition of saponin, using confocal microscopy (Figure S3). This data revealed that nuclear TDP-43^{WT}-tGFP remained bound within the nucleus of transfected cells throughout the 15 min incubation in saponin solution. This suggests that nuclear TDP-43 and cytoplasmic inclusions containing TDP-43 are indistinguishable at the imaging resolution of the automated

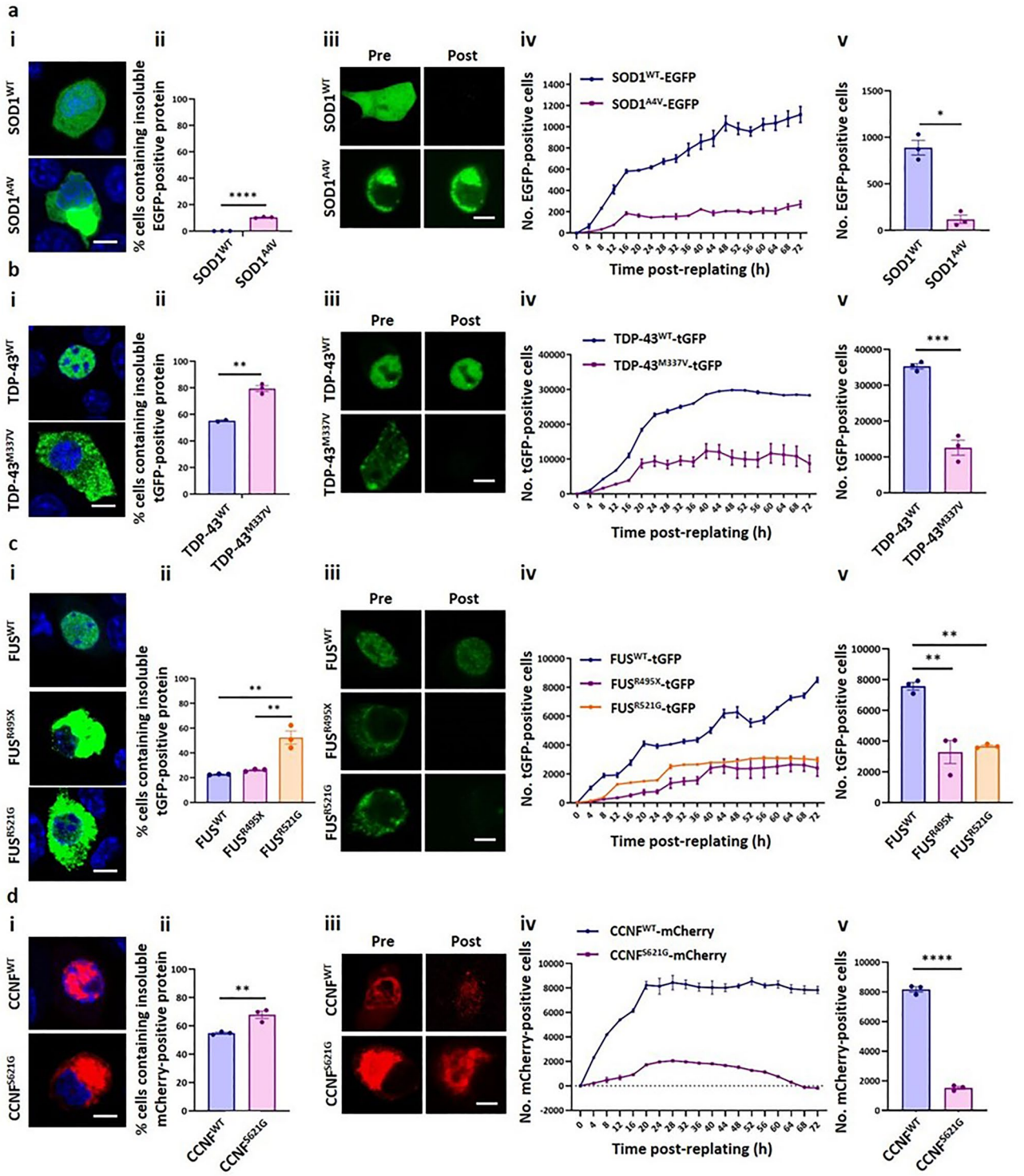

Figure 2. Characterising the localisation patterns and intracellular solubility of ALS-associated SOD1^{A4V}, TDP-43^{M337V}, FUS^{R495X}, FUS^{R521G} and CCNF^{S621G}. NSC-34 cells were transiently transfected with (**a**) SOD1^{WT}-EGFP or SOD1^{A4V}-EGFP, (**b**) TDP-43^{WT}-tGFP or TDP-43^{M337V}-tGFP, (**c**) FUS^{WT}-tGFP, FUS^{R495X}-tGFP or FUS^{R521G}-tGFP or (**d**) CCNF^{WT}-mCherry or CCNF^{S621G}-mCherry. After 48 h, transfected cells were either **(i)** fixed, nuclei stained with Hoechst and imaged using a Leica SP8 confocal microscope, **(ii** and **iii)** imaged on an IncuCyte® ZOOM, followed by incubation with 0.03% (w/v) saponin in PBS for 10 min at room temperature, before being imaged again on the IncuCyte or (iv and v) imaged in an IncuCyte® ZOOM over 72 h. **(i)** Representative images from confocal microscopy of Hoechst-stained cells. **(ii)** Cells were transfected in quadruplicate, and the data presented is the mean ± SEM of the percentage of transfected NSC-34 cells containing insoluble EGFP-/tGFP-/mCherry-positive protein following permeabilisation with saponin. **(iii)** Representative confocal images of cells prior to the addition of saponin solution ("Pre"), and following 10 min incubation in saponin solution ("Post"). **(iv)** Numbers of EGFP/tGFP/mCherry-positive cells over 72 h and **(v)** the mean ± SEM numbers of positive cells at 48 h post-replating, in triplicate wells of cells. Differences between the means were determined using Student's t test or One-Way ANOVA followed by Tukey's Multiple Comparison Test. * indicates $p < 0.05$, ** indicates $p < 0.01$, *** indicates $p < 0.001$ and **** indicates $p < 0.0001$. Scale bars represent 10 µm.

saponin-permeabilisation assay described here, and thus that this assay is not suitable for quantifying TDP-43 aggregation. However, addition of RNAse and DNAse to TDP-43-transfected cells may allow usage of this assay.

Similarly, while FUS^{WT}-tGFP was not observed to mislocalise and accumulate into cytoplasmic inclusions when transfected cells were examined using confocal microscopy, the saponin-permeabilisation assay quantified that FUS^{WT}-tGFP remained in 22.72 ± 0.25% of cells following incubation with saponin solution (Fig. 2c, ii). Moreover, the percentage of cells expressing FUS^{R495X}-tGFP that remained tGFP-positive following permeabilisation (26.15 ± 0.56%) was similar to that of cells expressing FUS^{WT}-tGFP. However, there was a significantly greater percentage of cells expressing FUS^{R521G}-tGFP that remained tGFP-positive (52.4 ± 5.29%) compared to both cells expressing FUS^{WT}-tGFP and cells expressing FUS^{R495X}-tGFP (FUS^{WT}-tGFP, $p = 0.0012$; FUS^{R495X}-tGFP, $p = 0.0023$). As noted above, when cells expressing the FUS-tGFP constructs were examined using confocal microscopy, there was extensive formation of small foci (< 2 µm) and large aggregates by both FUS mutants (Fig. 2c, i). Thus, the similar percentages of cells expressing FUS^{WT}-tGFP and FUS^{R495X}-tGFP that remained tGFP-positive after saponin-permeabilisation compared to the marked differences in their localisation patterns indicates that the saponin-permeabilisation assay may not be appropriate for quantifying the formation of insoluble cytoplasmic mutant FUS-tGFP inclusions. Indeed, similar to TDP-43, RNA-binding prevents FUS from exiting the nucleus and to be retained in cells, even when the plasma membrane has been compromised[63,64].

Since the original identification of the *CCNF*^{S621G} mutation in ALS and frontotemporal dementia patients[37], the localisation patterns of $CCNF^{S621G}$ in motor neurons have not been investigated in detail. However, Lee et al.[65] observed $CCNF^{S621G}$ localised to inclusion-like structures while $CCNF^{WT}$ displayed diffuse distribution. We observed mCherry-tagged $CCNF^{WT}$ fluorescence with diffuse distribution and predominant nuclear localisation in all imaged cells (Fig. 2d, i). In contrast, $CCNF^{S621G}$-mCherry formed into large amorphous aggregates ranging from 5 to > 10 µm. Saponin-permeabilisation assay data would suggest that that both $CCNF^{WT}$-mCherry and $CCNF^{S621G}$-mCherry formed extensively into insoluble structures, with > 50% of both cells transfected with $CCNF^{WT}$-mCherry cells and $CCNF^{S621G}$-mCherry cells containing insoluble mCherry-positive protein (Fig. 2d, ii). However, similar to nuclear WT TDP-43 and FUS, nuclear CCNF remains in cells following saponin-permeabilisation (Fig. 2d, iii), and suggests that the mCherry signal remaining in cells is detected and erroneously counted as insoluble intracellular inclusions by the automated imaging analysis pipeline of the saponin-permeabilisation assay. Nevertheless, there were significantly more $CCNF^{S621G}$-mCherry-expressing cells containing insoluble mCherry-positive protein (67.84 ± 2.61%) than there were of $CCNF^{WT}$-mCherry cells (54.89 ± 0.64%) ($p = 0.0085$).

HCA assay for proteostasis stress in cells expressing $SOD1^{A4V}$ and $CCNF^{S621G}$

The optimised HCA SpotDetector BioApplication was used to compare the effect of SOD1 and CCNF variant overexpression on the ability of the cellular protein quality control network to prevent aggregation of conformationally-destabilised, aggregation-prone Fluc mutants[66–70]. Fluc is a ~ 60 kDa multidomain protein that is known to be chaperone-dependent for folding and refolding[66–70]. It was reasoned that reductions in protein quality control network capacity would lead to increased aggregation of the EGFP-tagged Fluc mutants, as has been shown before[66].

To ensure that the SpotDetector BioApplication was capable of identifying and analysing transfected cells and fluorescent foci reliably and accurately, images from each experimental condition were manually examined (Fig. 3). While in some images transfected cells were occasionally not detected by the BioApplication, > 90% of ECFP- and EGFP-positive cells were detected (green circular masks). 'Spot' masks (yellow masks) were observed only on large foci with high fluorescence intensity, corresponding to the inclusion size and fluorescence intensity cut-offs established during assay optimisation.

Proteasome inhibition of cells expressing mCherry alone confirmed that increased proteome stress results in increased aggregation of the Fluc-EGFP isoforms. Cells expressing mCherry that were treated with MG132 developed significantly greater numbers of $Fluc^{WT}$-EGFP ($p < 0.0001$), $Fluc^{SM}$-EGFP ($p < 0.0001$) and $Fluc^{DM}$-EGFP ($p < 0.0001$) aggregates compared to untreated cells (Fig. 4a, i). MG132 treatment resulted in significantly higher numbers of $Fluc^{WT}$-EGFP aggregates than $Fluc^{DM}$-EGFP aggregates ($p = 0.0153$). $Fluc^{WT}$-EGFP aggregates were significantly smaller ($p = 0.002$) and more brightly fluorescent ($p < 0.0001$) than $Fluc^{DM}$-EGFP aggregates (Fig. 4b, i and c, i). Aggregates of the Fluc-EGFP isoforms were also detected in cells expressing SOD1-tdT, with a significant increase in the numbers of aggregates formed in cells expressing $SOD1^{A4V}$-tdT compared to $SOD1^{WT}$-tdT ($Fluc^{WT}$-EGFP, $p = 0.0331$; $Fluc^{SM}$-EGFP, $p = 0.0061$; $Fluc^{DM}$-EGFP, $p = 0.0042$) (Fig. 4a, ii). There were also increases in the mean size of $Fluc^{DM}$-EGFP aggregates ($p = 0.0430$) and fluorescence intensity of aggregates of $Fluc^{WT}$-EGFP ($p < 0.0001$), $Fluc^{SM}$-EGFP ($p < 0.0001$) and $Fluc^{DM}$-EGFP ($p < 0.0001$) in cells expressing $SOD1^{A4V}$-tdT compared to $SOD1^{WT}$-tdT (Fig. 4b, ii and c, ii). Interestingly, aggregation of $Fluc^{SM}$-EGFP and $Fluc^{DM}$-EGFP was as extensive in cells expressing $CCNF^{WT}$-mCherry as those expressing $CCNF^{S621G}$-mCherry (Fig. 4a, iii). Whilst aggregates of $Fluc^{WT}$-EGFP were also detected, there were significantly lower numbers of cells containing them compared to the numbers of cells containing aggregates of $Fluc^{SM}$-EGFP ($p < 0.001$) and $Fluc^{DM}$-EGFP ($p < 0.0001$), both in cells expressing $CCNF^{WT}$-mCherry and cells expressing $CCNF^{S621G}$-mCherry. There was also the same trend in the size of aggregates of the Fluc-EGFP isoforms in cells expressing $CCNF^{WT}$-mCherry and those expressing $CCNF^{S621G}$-mCherry, with significantly larger aggregates of $Fluc^{DM}$-EGFP formed than aggregates of $Fluc^{WT}$-EGFP ($CCNF^{WT}$-mCherry, $p = 0.0395$; $CCNF^{S621G}$-mCherry, $p = 0.0328$) (Fig. 4b, iii). There was no difference in the mean fluorescence intensity of the Fluc-EGFP aggregates of the Fluc-EGFP isoforms between cells expressing $CCNF^{WT}$-mCherry and cells expressing $CCNF^{S621G}$-mCherry (Fig. 4c, iii).

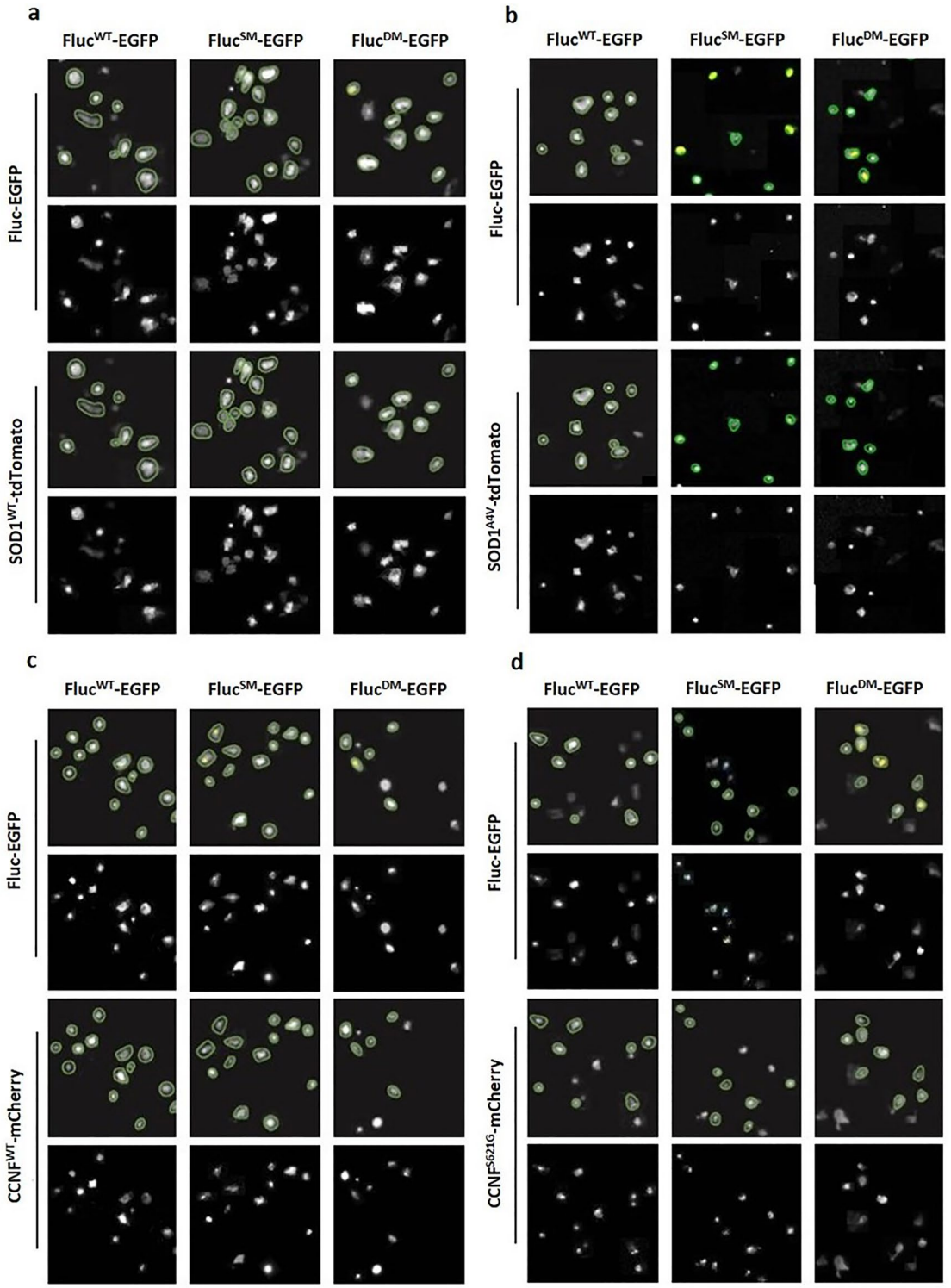

Figure 3. Optimisation of High Content Analysis of Fluc-EGFP foci in transfected cells. Representative Cellomics® ArrayScan™ VTI images showing SpotDetector BioApplication masks (first and third rows of each panel) used to identify and select NSC-34 cells co-transfected with either (**a**) $SOD1^{WT}$-tdTomato, (**b**) $SOD1^{A4V}$-tdTomato, (**c**) $CCNF^{WT}$-mCherry or (**d**) $CCNF^{S621G}$-mCherry and $Fluc^{WT}$-EGFP, $Fluc^{SM}$-EGFP or $Fluc^{DM}$-EGFP. Cells were imaged at 48 h post-transfection. Green circular masks indicate cells selected for analysis, yellow masks indicate 'spots' selected for analysis, representing aggregates. Images were acquired using a 20 × objective lens.

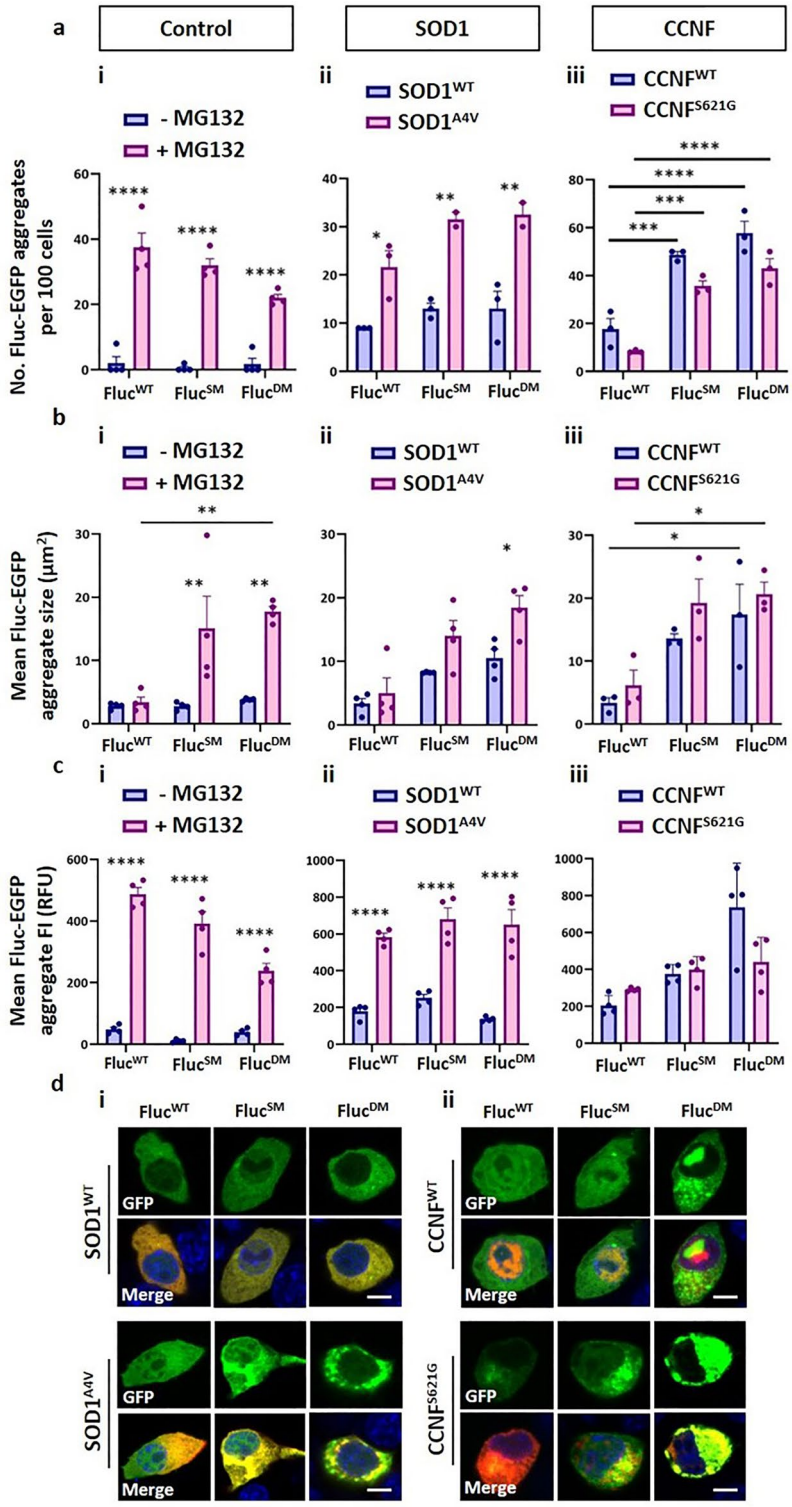

Figure 4. HCA analysis of Firefly luciferase mutants reports on chaperone network activity in NSC-34 cells expressing SOD1 and CCNF. (**a**) Numbers of Fluc-EGFP aggregates per 100 transfected cells, (**b**) mean size of Fluc-EGFP aggregates (μm^2) and (**c**) mean fluorescence intensity (FI) of Fluc-EGFP aggregates imaged at 48 h post-transfection in NSC-34 cells expressing $Fluc^{WT}$-EGFP, $Fluc^{SM}$-EGFP or $Fluc^{DM}$-EGFP with **(i)** mCherry alone ± treatment with 5 μM MG132, **(ii)** $SOD1^{WT}$-tdTomato or $SOD1^{A4V}$-tdTomato or **(iii)** $CCNF^{WT}$-mCherry or $CCNF^{S621G}$-mCherry. Treatment with MG132 was carried out at 30 h post-transfection. For mock treatment, 5 μM DMSO was instead added to cells. Graphs represent the mean ± SEM from quadruplicate wells of cells in n = 1 experiment, analysed using Cellomics® ArrayScan™ VTI and SpotDetector BioApplication. Differences between the means were determined using One-Way ANOVA followed by Tukey's Multiple Comparison Test. * indicates $p < 0.05$, ** indicates $p < 0.01$, *** indicates $p < 0.001$, **** indicates $p < 0.0001$. (**d**) Representative confocal images of Hoechst-stained NSC-34 cells expressing $Fluc^{WT}$-EGFP, $Fluc^{SM}$-EGFP or $Fluc^{DM}$-EGFP with **(i)** $SOD1^{WT}$-tdTomato or $SOD1^{A4V}$-tdTomato or **(ii)** $CCNF^{WT}$-mCherry or $CCNF^{S621G}$-mCherry. Scale bars represent 10 μm.

Discussion

The genetic heterogeneity of ALS distinguishes it from most other neurodegenerative diseases, which can be linked to a limited number of pathogenic mechanisms and phenotypes. The ALS research field would benefit greatly from the use of experimental systems with HCA capacity to help navigate through the complexity of ALS. To address this, we have developed an HCA methodology to use with cellular ALS models. The overall objective of this work was to develop a system that could be used to collect descriptive phenotypic data from cellular ALS models that would enable (1) characterisation of the inclusion formation pathways of different ALS-associated proteins, and (2) the use of diverse markers of proteome stress and motor neuron dysfunction to assess potential therapeutic compounds and genetic modifiers of ALS disease mechanisms and toxicity.

The NSC-34 models of ALS generated here were examined for the localisation, mobility and solubility of the fusion proteins. The aim of these studies was to establish disease phenotypes that could be used in an experimental system with HCA capacity for further studies into disease mechanisms, and potentially for evaluation of candidate therapeutics. This HCA experimental system was generated through optimising the SpotDetector BioApplication to investigate reductions in cellular protein folding/re-folding capacity caused by WT and mutant SOD1 and CCNF. Analysis was facilitated by co-expression of conformationally-destablised Fluc-EGFP mutants[66] with WT and mutant SOD1 and CCNF. We hypothesised that dysregulation of proteostasis mechanisms that may be exacerbated by ALS-associated mutations would overload cellular proteostasis capacity, resulting in inability of the cellular pool of molecular chaperones to prevent aggregation of the Fluc-EGFP mutants. The optimised SpotDetector BioApplication enabled quantification of the numbers, mean size and fluorescence intensity of aggregates formed by the Fluc-EGFP isoforms.

The ability of the Fluc-EGFP mutants to report on proteome stress was confirmed through proteasome inhibition of cells expressing mCherry alone. In MG132-treated cells, $Fluc^{WT}$-EGFP aggregates that formed were smaller than the aggregates formed by $Fluc^{SM}$-EGFP and $Fluc^{DM}$-EGFP, indicating that less of the WT protein misfolded and accumulated into aggregates. Without exogenous proteome stress induced by proteasome inhibition, there was negligible aggregation of the Fluc-EGFP isoforms, demonstrating that they were able to report on increased proteome stress.

The data from the present work demonstrates that the optimised Fluc-EGFP HCA assay is able to report on reduced activity of the chaperone network resulting from the expression of $SOD1^{A4V}$ as previously reported[25,71,72]. The overexpression of $CCNF^{WT}$-mCherry caused the same extent of Fluc-EGFP aggregation as $CCNF^{S621G}$-mCherry, indicating that mutant CCNF did not differentially affect chaperone activity compared to $CCNF^{WT}$. CCNF is an important protein in the ubiquitin–proteasome system, as a mediator of protein ubiquitylation[73]. Ubiquitylation of target proteins is altered in cells expressing mutant CCNF, causing aberrant accumulation of ubiquitylated proteins and consequent stress on the proteostasis network[37]. The data obtained from the Fluc-EGFP HCA assay developed in the present work suggests that proteostasis disruption caused by mutant CCNF does not involve impairment of the protein folding/re-folding activity of chaperones.

The Fluc-EGFP isoforms were designed to act as sensors of cellular protein folding/re-folding capacity that would themselves have minimal biological impact in most of the commonly used cellular and animal models[66]. In the present work it was demonstrated that they are suitable for use in an HCA assay format to report on disruptions in the activity of the cellular chaperone network. In future work it would be useful to optimise an HCA assay that utilises changes in luminescence activity of the Fluc-EGFP isoforms[66] as an additional measure.

In addition to the use of this Fluc-EGFP HCA assay to examine cellular models of $SOD1^{A4V}$ and $CCNF^{S621G}$, it would be useful in future work to utilise this assay to examine the cellular models of mutant TDP-43, FUS, UBQLN2, OPTN, VAPB and VCP generated in this work. Beyond establishing ALS-associated mutant proteins that impair the activity of the chaperone network in cells, this HCA assay could have potential for application in studies to screen for drugs that ameliorate chaperone activity impairment.

Data availability

The datasets generated and analysed during the current study are available from the corresponding author on reasonable request.

Received: 22 November 2021; Accepted: 7 June 2024
Published online: 15 June 2024

References

1. Mackenzie, I. R. *et al.* Pathological TDP-43 distinguishes sporadic amyotrophic lateral sclerosis from amyotrophic lateral sclerosis with SOD1 mutations. *Ann. Neurol.* **61**(5), 427–434 (2007).
2. Kwong, L. K., Neumann, M., Sampathu, D. M., Lee, V. M. & Trojanowski, J. Q. TDP-43 proteinopathy: The neuropathology underlying major forms of sporadic and familial frontotemporal lobar degeneration and motor neuron disease. *Acta Neuropathol.* **114**(1), 63–70 (2007).
3. Kwiatkowski, T. J. Jr. *et al.* Mutations in the FUS/TLS gene on chromosome 16 cause familial amyotrophic lateral sclerosis. *Science* **323**(5918), 1205–1208 (2009).
4. Vance, C. *et al.* Mutations in FUS, an RNA processing protein, cause familial amyotrophic lateral sclerosis type 6. *Science* **323**(5918), 1208–1211 (2009).
5. Bolognesi, B. *et al.* ANS binding reveals common features of cytotoxic amyloid species. *ACS Chem. Biol.* **5**(8), 735–740 (2010).
6. Proctor, E. A. *et al.* Nonnative SOD1 trimer is toxic to motor neurons in a model of amyotrophic lateral sclerosis. *Proc. Natl. Acad. Sci. U S A.* **113**(3), 614–619 (2016).
7. Zhu, C., Beck, M. V., Griffith, J. D., Deshmukh, M. & Dokholyan, N. V. Large SOD1 aggregates, unlike trimeric SOD1, do not impact cell viability in a model of amyotrophic lateral sclerosis. *Proc. Natl. Acad. Sci. U S A.* **115**(18), 4661–4665 (2018).
8. Johnston, J. A., Ward, C. L. & Kopito, R. R. Aggresomes: A cellular response to misfolded proteins. *J Cell Biol.* **143**(7), 1883–1898 (1998).
9. Kopito, R. R. Aggresomes, inclusion bodies and protein aggregation. *Trends Cell Biol.* **10**(12), 524–530 (2000).

10. Kawaguchi, Y. *et al.* The deacetylase HDAC6 regulates aggresome formation and cell viability in response to misfolded protein stress. *Cell* **115**(6), 727–738 (2003).
11. Arrasate, M., Mitra, S., Schweitzer, E. S., Segal, M. R. & Finkbeiner, S. Inclusion body formation reduces levels of mutant huntingtin and the risk of neuronal death. *Nature* **431**(7010), 805–810 (2004).
12. Kaganovich, D., Kopito, R. & Frydman, J. Misfolded proteins partition between two distinct quality control compartments. *Nature* **454**(7208), 1088–1095 (2008).
13. Tan, J. M. *et al.* Lysine 63-linked ubiquitination promotes the formation and autophagic clearance of protein inclusions associated with neurodegenerative diseases. *Hum. Mol. Genet.* **17**(3), 431–439 (2008).
14. Treusch, S., Cyr, D. M. & Lindquist, S. Amyloid deposits: Protection against toxic protein species?. *Cell Cycle* **8**(11), 1668–1674 (2009).
15. Zhang, X. & Qian, S. B. Chaperone-mediated hierarchical control in targeting misfolded proteins to aggresomes. *Mol. Biol. Cell* **22**(18), 3277–3288 (2011).
16. Weisberg, S. J. *et al.* Compartmentalization of superoxide dismutase 1 (SOD1G93A) aggregates determines their toxicity. *Proc. Natl. Acad. Sci. U S A.* **109**(39), 15811–15816 (2012).
17. Polling, S. *et al.* Misfolded polyglutamine, polyalanine, and superoxide dismutase 1 aggregate via distinct pathways in the cell. *J. Biol. Chem.* **289**(10), 6669–6680 (2014).
18. Grad, L. I. *et al.* Intercellular propagated misfolding of wild-type Cu/Zn superoxide dismutase occurs via exosome-dependent and -independent mechanisms. *Proc. Natl. Acad. Sci. U S A.* **111**, 3620 (2014).
19. McAlary, L., Plotkin, S. S., Yerbury, J. J. & Cashman, N. R. Prion-like propagation of protein misfolding and aggregation in amyotrophic lateral sclerosis. *Front. Mol. Neurosci.* https://doi.org/10.3389/fnmol.2019.00262 (2019).
20. Yerbury, J. J. *et al.* Walking the tightrope: Proteostasis and neurodegenerative disease. *J. Neurochem.* **137**(4), 489–505 (2016).
21. Yerbury, J. J., Farrawell, N. E. & McAlary, L. Proteome homeostasis dysfunction: A unifying principle in ALS pathogenesis. *Trends Neurosci.* **43**(5), 274–284 (2020).
22. Lambert-Smith, I. A., Saunders, D. N. & Yerbury, J. J. Proteostasis impairment and ALS. *Prog. Biophys. Mol. Biol.* **174**, 3–27 (2022).
23. Rosen, D. R. *et al.* Mutations in Cu/Zn superoxide dismutase gene are associated with familial amyotrophic lateral sclerosis. *Nature* **362**(6415), 59–62 (1993).
24. Watanabe, M. *et al.* Histological evidence of protein aggregation in mutant SOD1 transgenic mice and in amyotrophic lateral sclerosis neural tissues. *Neurobiol. Dis.* **8**(6), 933–941 (2001).
25. Takeuchi, H. *et al.* Hsp70 and Hsp40 improve neurite outgrowth and suppress intracytoplasmic aggregate formation in cultured neuronal cells expressing mutant SOD1. *Brain Res.* **949**(1–2), 11–22 (2002).
26. Cheroni, C. *et al.* Accumulation of human SOD1 and ubiquitinated deposits in the spinal cord of SOD1G93A mice during motor neuron disease progression correlates with a decrease of proteasome. *Neurobiol. Dis.* **18**(3), 509–522 (2005).
27. Matsumoto, G., Stojanovic, A., Holmberg, C. I., Kim, S. & Morimoto, R. I. Structural properties and neuronal toxicity of amyotrophic lateral sclerosis–associated Cu/Zn superoxide dismutase 1 aggregates. *J. Cell Biol.* **171**(1), 75–85 (2005).
28. Cheroni, C. *et al.* Functional alterations of the ubiquitin-proteasome system in motor neurons of a mouse model of familial amyotrophic lateral sclerosis. *Hum. Mol. Genet.* **18**(1), 82–96 (2009).
29. Crippa, V. *et al.* The small heat shock protein B8 (HspB8) promotes autophagic removal of misfolded proteins involved in amyotrophic lateral sclerosis (ALS). *Hum. Mol. Genet.* **19**(17), 3440–3456 (2010).
30. Urushitani, M., Kurisu, J., Tsukita, K. & Takahashi, R. Proteasomal inhibition by misfolded mutant superoxide dismutase 1 induces selective motor neuron death in familial amyotrophic lateral sclerosis. *J. Neurochem.* **83**(5), 1030–1042 (2002).
31. Watts, G. D. *et al.* Inclusion body myopathy associated with Paget disease of bone and frontotemporal dementia is caused by mutant valosin-containing protein. *Nat. Genet.* **36**(4), 377–381 (2004).
32. Johnson, J. O. *et al.* Exome sequencing reveals VCP mutations as a cause of familial ALS. *Neuron* **68**(5), 857–864 (2010).
33. Deng, H. X. *et al.* Mutations in UBQLN2 cause dominant X-linked juvenile and adult-onset ALS and ALS/dementia. *Nature* **477**(7363), 211–215 (2011).
34. Maruyama, H. *et al.* Mutations of optineurin in amyotrophic lateral sclerosis. *Nature* **465**(7295), 223–226 (2010).
35. Kamada, M. *et al.* Clinicopathologic features of autosomal recessive amyotrophic lateral sclerosis associated with optineurin mutation. *Neuropathology* **34**(1), 64–70 (2014).
36. Nishimura, A. L. *et al.* A mutation in the vesicle-trafficking protein VAPB causes late-onset spinal muscular atrophy and amyotrophic lateral sclerosis. *Am. J. Hum. Genet.* **75**(5), 822–831 (2004).
37. Williams, K. L. *et al.* CCNF mutations in amyotrophic lateral sclerosis and frontotemporal dementia. *Nat. Commun.* **7**, 11253 (2016).
38. Neumann, M. *et al.* Ubiquitinated TDP-43 in frontotemporal lobar degeneration and amyotrophic lateral sclerosis. *Science* **314**(5796), 130–133 (2006).
39. Sreedharan, J. *et al.* TDP-43 mutations in familial and sporadic amyotrophic lateral sclerosis. *Science* **319**(5870), 1668–1672 (2008).
40. Turner, M. R. *et al.* Controversies and priorities in amyotrophic lateral sclerosis. *Lancet Neurol.* **12**(3), 310–322 (2013).
41. Farrawell, N. *et al.* Distinct partitioning of ALS associated TDP-43, FUS and SOD1 mutants into cellular inclusions. *Sci. Rep.* **5**(13416), 1–14 (2015).
42. Hoell, J. I. *et al.* RNA targets of wild-type and mutant FET family proteins. *Nat. Struct. Mol. Biol.* **18**(12), 1428–1431 (2011).
43. Polymenidou, M. *et al.* Long pre-mRNA depletion and RNA missplicing contribute to neuronal vulnerability from loss of TDP-43. *Nat. Neurosci.* **14**(4), 459–468 (2011).
44. Tollervey, J. R. *et al.* Characterizing the RNA targets and position-dependent splicing regulation by TDP-43. *Nat. Neurosci.* **14**(4), 452–458 (2011).
45. Colombrita, C. *et al.* TDP-43 and FUS RNA-binding proteins bind distinct sets of cytoplasmic messenger RNAs and differently regulate their post-transcriptional fate in motoneuron-like cells. *J. Biol. Chem.* **287**(19), 15635–15647 (2012).
46. Lagier-Tourenne, C. *et al.* Divergent roles of ALS-linked proteins FUS/TLS and TDP-43 intersect in processing long pre-mRNAs. *Nat. Neurosci.* **15**(11), 1488–1497 (2012).
47. Voigt, A. *et al.* TDP-43-mediated neuron loss in vivo requires RNA-binding activity. *PLoS One* **5**(8), e12247 (2010).
48. Cashman, N. R. *et al.* Neuroblastoma x spinal cord (NSC) hybrid cell lines resemble developing motor neurons. *Dev. Dynam.* **194**, 209 (1992).
49. Deng, H. X. *et al.* Amyotrophic lateral sclerosis and structural defects in Cu,Zn superoxide dismutase. *Science* **261**(5124), 1047 (1993).
50. Tamaoka, A. *et al.* TDP-43 M337V mutation in familial amyotrophic lateral sclerosis in Japan. *Intern. Med.* **49**(4), 331–334 (2010).
51. Shibata, N. *et al.* Cu/Zn superoxide dismutase-like immunoreactivity in Lewy body-like inclusions of sporadic amyotrophic lateral sclerosis. *Neurosci. Lett.* **179**(1–2), 149–152 (1994).
52. Leigh, P. N. *et al.* Ubiquitin-immunoreactive intraneuronal inclusions in amyotrophic lateral sclerosis. Morphology, distribution, and specificity. *Brain* **114**(2), 775–788 (1991).
53. Strong, M. J., Kesavapany, S. & Pant, H. C. The pathobiology of amyotrophic lateral sclerosis: A proteinopathy?. *J. Neuropathol. Exp. Neurol.* **64**(8), 649–664 (2005).
54. Teyssou, E. *et al.* Mutations in SQSTM1 encoding p62 in amyotrophic lateral sclerosis: Genetics and neuropathology. *Acta Neuropathol.* **125**(4), 511–522 (2013).

55. Matsumoto, G., Kim, S. & Morimoto, R. I. Huntingtin and mutant SOD1 form aggregate structures with distinct molecular properties in human cells. *J. Biol. Chem.* **281**(7), 4477–4485 (2006).
56. Johnston, J. A. Formation of high molecular weight complexes of mutant. *Proc. Natl. Acad. Sci.* **97**(23), 12571–12576 (2000).
57. Cozzolino, M. Cysteine 111 affects aggregation and cytotoxicity of mutant Cu, Zn-superoxide dismutase associated with familial amyotrophic lateral sclerosis. *J. Biol. Chem.* **283**(2), 866–874 (2008).
58. Kuijpers, M. *et al.* Amyotrophic lateral sclerosis (ALS)-associated VAPB-P56S inclusions represent an ER quality control compartment. *Acta Neuropathol. Commun.* **1**, 24 (2013).
59. Zeineddine, R. *et al.* SOD1 protein aggregates stimulate macropinocytosis in neurons to facilitate their propagation. *Mol. Neurodegener.* **10**(1), 57 (2015).
60. Pokrishevsky, E. *et al.* Tryptophan 32-mediated SOD1 aggregation is attenuated by pyrimidine-like compounds in living cells. *Sci. Rep.* **8**(1), 15590 (2018).
61. Ederle, H. *et al.* Nuclear egress of TDP-43 and FUS occurs independently of exportin-1/CRM1. *Sci. Rep.* **8**(1), 7084 (2018).
62. Duan, L. *et al.* Nuclear RNA binding regulates TDP-43 nuclear localization and passive nuclear export. *Cell Rep.* **40**(3), 111106 (2022).
63. Baade, I. *et al.* The RNA-binding protein FUS is chaperoned and imported into the nucleus by a network of import receptors. *J. Biol. Chem.* **296**, 100659 (2021).
64. Tsai, Y.-L., Mu, Y. C. & Manley, J. L. Nuclear RNA transcript levels modulate nucleocytoplasmic distribution of ALS/FTD-associated protein FUS. *Sci. Rep.* **12**(1), 8180 (2022).
65. Lee, A. *et al.* Pathogenic mutation in the ALS/FTD gene, CCNF, causes elevated Lys48-linked ubiquitylation and defective autophagy. *Cell. Mol. Life Sci.* **75**(2), 335–354 (2018).
66. Gupta, R. *et al.* Firefly luciferase mutants as sensors of proteome stress. *Nat. Methods* **8**(10), 879–884 (2011).
67. Frydman, J., Nimmesgern, E., Ohtsuka, K. & Hartl, F. U. Folding of nascent polypeptide chains in a high molecular mass assembly with molecular chaperones. *Nature* **370**(6485), 111–117 (1994).
68. Thulasiraman, V. & Matts, R. L. Effect of geldanamycin on the kinetics of chaperone-mediated renaturation of firefly luciferase in rabbit reticulocyte lysate. *Biochemistry* **35**(41), 13443–13450 (1996).
69. Nimmesgern, E. & Hartl, F. U. ATP-dependent protein refolding activity in reticulocyte lysate. Evidence for the participation of different chaperone components. *FEBS Lett.* **331**(1–2), 25–30 (1993).
70. Schroder, H., Langer, T., Hartl, F. U. & Bukau, B. DnaK, DnaJ and GrpE form a cellular chaperone machinery capable of repairing heat-induced protein damage. *Embo J.* **12**(11), 4137–4144 (1993).
71. Tummala, H. *et al.* Inhibition of chaperone activity is a shared property of several Cu, Zn-superoxide dismutase mutants that cause amyotrophic lateral sclerosis. *J. Biol. Chem.* **280**(18), 17725–17731 (2005).
72. Bruening, W. *et al.* Up-regulation of protein chaperones preserves viability of cells expressing toxic Cu/Zn-superoxide dismutase mutants associated with amyotrophic lateral sclerosis. *J. Neurochem.* **72**(2), 693–699 (1999).
73. D'Angiolella, V., Esencay, M. & Pagano, M. A cyclin without cyclin-dependent kinases: Cyclin F controls genome stability through ubiquitin-mediated proteolysis. *Trends Cell Biol.* **23**(3), 135–140 (2013).

Author contributions

Isabella A. Lambert-Smith: conceptualisation, methodology, validation, formal analysis, investigation, data curation, writing—original draft, visualisation. Victoria K. Shephard: investigation, data curation, validation. Luke McAlary: writing—review & editing, supervision. Justin J. Yerbury: conceptualisation, methodology, formal analysis, investigation, resources, writing—review & editing, visualisation, supervision, project administration, funding acquisition. Darren N. Saunders: conceptualisation, methodology, formal analysis, investigation, resources, writing—review & editing, visualisation, supervision, project administration, funding acquisition.

Funding

J.J.Y. was supported by a University of Wollongong Professorship in Neurodegenerative Diseases, and by a National Health and Medical Research Council, Australia Dementia Teams Grant (1095215) and Investigator Grant (1194872). L.M. was supported by the MNDRA Bill Gole Fellowship and acknowledges funding from FightMND.

Competing interests

The authors declare that the research was conducted in the absence of any commercial, financial or non-financial relationships that could be construed as potential competing interests.

Additional information

Supplementary Information The online version contains supplementary material available at https://doi.org/10.1038/s41598-024-64366-0.

Correspondence and requests for materials should be addressed to I.A.L.-S. or D.N.S.

Reprints and permissions information is available at www.nature.com/reprints.

Publisher's note Springer Nature remains neutral with regard to jurisdictional claims in published maps and institutional affiliations.